Journal of Organometallic Chemistry 887 (2019) 48–63

Contents lists available at ScienceDirect

Journal of Organometallic Chemistry

journal homepage: www.elsevier.com/locate/jorganchem

Synthesis and comparative studies of photophysical and electrochemical properties of three different types of new heteroleptic 5-arylazo-8-hydroxyquinoline complexes of rhodium including trans → *cis* isomerism studies

Amit Maity, Sachinath Bera, Kajal Krishna Rajak*

Inorganic Chemistry Section, Department of Chemistry, Jadavpur University, Kolkata, 700032, India

ARTICLE INFO

Article history:
Received 16 November 2018
Received in revised form
1 February 2019
Accepted 12 February 2019
Available online 2 March 2019

Keywords:
rhodium(III) complexes
Comparative photophysical studies
DFT and TDDFT studies
Cis-trans isomerism studies

ABSTRACT

Refluxing $[Rh(2\text{-phpy})_2(Cl)]_2$ separately with the equivalent amount of 5-phenylazo-8-hydroxyquinoline (Hq^1), 5-(4-fluorophenylazo)-8-hydroxyquinoline (Hq^2) and 5-(4-nitrophenylazo)-8-hydroxyquinoline (Hq^3) in toluene in aerobic condition afforded mononuclear orange coloured compounds having general formula $[Rh(2\text{-phpy})_2(q)]$ in excellent yields. The complexes were substantiated by IR, ^1H NMR, ESI-mass, EPR, UV–Vis and emission spectra, cyclic voltammetry, single-crystal X-ray structure determinations and density functional theory (DFT) calculations. Synthesis and comparison of their photophysical and electrochemical properties of a new branch of rhodium(III) complexes of 8-hydroxyarylazo analogues are presented which are never studied before. The ground and excited-state geometries, absorption, and emission properties of the complexes were examined by DFT and TDDFT methods. The excitations and emissions are investigated by the natural transition orbital (NTO) analysis. The emission occurred via ^{3}MLCT or ^{3}ILCT transition by theoretical analysis of triplet state DFT calculations. The *cis*-trans isomerism studies for the azo complexes have been done by experimental as well as theoretical analysis.

1. Introduction

The studies of transition metal complexes especially iridium and rhodium complexes exhibiting highly efficient room-temperature phosphorescence properties are main interest [1–4]. Especially, the rhodium(III) complexes are to be considered as a promising member due to their unique combination of chemical stability, strong visible absorption, excited state reactivity, photo redox chemistry and catalytic properties [5–12]. These properties of such complexes can be attributed to the moderate spin-orbit coupling provided by the rhodium(III) ion. The metal ligand interaction is a consequence of the triplet excited state of metal to ligand charge transfer which can emit molecular photoluminescence.

During the last few decades, a large number of reports have been published focusing to design and characterize the luminescent metal complexes bearing 8-hydroxyquinoline and their derivatives as ligands [13–17]. 8-Hydroxyquinoline derivatives are of particular interest because of the possibility of tuning the energy gap by the simple attachment of electron-donating or electron-withdrawing groups and the commercial availability of many 8-hydroxyquinoline derivatives. Although considerable scientific efforts have been given on studying luminescent metal complexes of aluminium, platinum, palladium or boron containing 8-hydroxyquinolines as ligands, the corresponding investigations on the impact of ligand modifications on the materials properties of cyclometalated organorhodium 8-hydroxyquinolinolate complexes are not well known.

Diverse functionalities of the metal complexes containing 8-hydroxyquinoline prompted us to design and synthesize new types of rhodium(III) complexes of 8-hydroxyquinolate with different ancillary ligands containing extended π-conjugation and analyze the light-harvesting capabilities in respect to both the molar extinction coefficient and the bathochromic shift of the absorption.

In this article, we report the syntheses, molecular structures and

* Corresponding author.
E-mail addresses: kajalrajak@rediffmail.com, kkrajak@chemistry.jdvu.ac.in (K.K. Rajak).

https://doi.org/10.1016/j.jorganchem.2019.02.012
0022-328X/

photo-physical properties of three new rhodium(III) complexes of the types $[Rh^{III}(2\text{-phpy})_2(q^1)]$ (**1**), $[Rh^{III}(2\text{-phpy})_2(q^2)]$ (**2**), and $[Rh^{III}(2\text{-phpy})_2(q^3)]$ (**3**) where Hq^1 = 5-phenylazo-8-hydroxyquinoline, Hq^2 = 5-(4-fluorophenylazo)-8-hydroxyquinoline and Hq^3 = 5-(4-nitrophenylazo)-8-hydroxyquinoline as shown in Chart 1. Evidently, we have introduced different arylazo moieties at the 5-position to Hq ligand in order to follow the nature the bathochromic shift of the MLCT absorption in the visible region. Here, we have demonstrated the variation of optical properties by changing the nature substitution at the 5-position of the attached aryl azo moiety. The complexes are characterized by IR, mass, UV–vis, ^{1}HNMR and EPR spectroscopy. The electrochemical behaviours are also examined by cyclic voltammetry study. Molecular geometries of the complexes were confirmed by single crystal X-ray structure determination. The complexes with the free azo ligand moiety may rotate against the azo bond to exhibit *cis*-trans isomerisation in presence of photonic irradiation. Upon irradiation with UV or blue light azobenzene derivatives [18–32] are known to undergo efficient *trans*-to-*cis* isomerisation, which can be reversed either photochemically or thermally. The thermodynamically less stable cis isomer can be achieved from more stable trans isomer by applying irradiation of UV light with specific wavelength and the reverse can also be achieved easily with few seconds by heating or visible light. All complexes are irradiated with the dichloromethane solution of the complexes by UV light of fixed wavelength and got some interesting results.

In recent years, with the development and improvement of density functional theory (DFT) and the time-dependent density functional theory (TDDFT) [33] the properties of both ground and excited-states of the metal complexes can be measured with good accuracy. By means of DFT calculations the geometry and the electronic structure geometry optimizations of the ground and excited-states were carried out to get the better result. We also designed and analyzed the singlet and triplet excited state natural transition orbitals (NTOs) obtained from TDDFT results and evaluate them with the ground state molecular orbitals (MOs) calculated by DFT calculations.

2. Experimental section

2.1. Materials

The solvents including dichloromethane, toluene, hexane, acetonitrile etc and chemicals including 2-phenylpyridine, 8-hydroxyquinoline etc which were used are analytically pure and high grade. Dimer, $[Rh^{III}(2\text{-phpy})_4Cl_2]$ compound was synthesized by following literature procedure [34].

2.2. Physical measurements

Elemental analyses (C, H, N) were performed on a Perkin–Elmer 2400 series II analyzer. Electrospray ionization mass spectrometry (ESI-MS) spectra were recorded on a Micromass QTOF YA 263 mass spectrometer. IR spectra were observed and obtained with a Perkin–Elmer L-0100 spectrophotometer with KBr disk. ^{1}H NMR spectra were measured on a Bruker FT 300 MHz spectrometer in $CDCl_3$ solvent. By Perkin–Elmer LAMBDA 25 spectrophotometer UV–Vis spectra were investigated. The emission data were collected on a Horiba FluroMax-4 fluorescence spectrometer. For all luminescence measurements slit width of 3 nm was used for both excitation and emission. By using CHI 620A electrochemical analyzer using platinum electrode electrochemical measurements were recorded under nitrogen atmosphere. Using freeze-pump-thaw-degassed solutions of the complexes by a relative method using quinine sulfate in the same solvent as the standard [Φ_{std} = 0.54 (at 298 K) in 0.1 M H_2SO_4 at λ_{ex} = 350 nm] by usual method quantum yields of the complexes were determined. The fluorescence life time was determined by usual method. The quantum yields were calculated using eq (1),

$$\Phi_r = \Phi_{std}\frac{A_{std}}{A_r}\frac{I_r}{I_{std}}\frac{\eta_r^2}{\eta_{std}^2} \quad (1)$$

where, Φ_r and Φ_{std} are the quantum yields of unknown and standard samples, A_r and A_{std} (<0.1) are the solution absorbance's at the excitation wavelength (λ_{ex}), I_r and I_{std} are the integrated emission intensities, and η_r and η_{std} are the refractive indices of the solvent. Time–correlated single–photon–counting (TCSPC) measurements were carried out for the luminescence decay of complexes in dichloromethane. On a Hamamatsu MCP photomultiplier (R3809) and were analyzed by using IBH DAS6 software, the fluorescence decay data were investigated.

2.3. Syntheses

(E)-5-(phenyldiazenyl)quinolin-8-ol (Hq^1), (E)-5-((4-fluorophenyl)diazenyl)quinolin-8-ol (Hq^2) and (E)-5-((4-nitrophenyl)diazenyl)quinolin-8-ol (Hq^3). The ligands Hq^1, Hq^2, and Hq^3 were prepared according to the literature procedure (general abbreviation Hq) [35].

$[Rh^{III}(2\text{-phpy})_2(q^1)]$ (1). A mixture of Hq^1 (50 mg, 0.20 mmol) and $[(2\text{-phpy})_2Rh(\mu\text{-Cl})]_2$ (150 mg, 0.20 mmol) in toluene (60 mL) was refluxed for 8 h. After cooling the solution to room temperature, the volume was reduced under reduced pressure to 6 ml. An orange precipitate was obtained after adding hexane about 18 ml. The precipitate was washed with ethanol and dried in air. On diffusion of hexane to the dichloromethane solution of the crude afforded orange coloured crystals of **1**. Yield: 130 mg (65%). $C_{37}H_{26}N_5ORh$: Elemental Anal. Calcd.: C, 67.38; H, 3.97; N, 10.62. Found: C, 63.52; H, 4.03; N, 10.64. ESI-MS (CH_2Cl_2): *m/z* 660.1246 $[M + H]^+$. IR_{exptl} (KBr, cm^{-1}) ν: 1460 (N=N), 1401, 1329, 1242; ^{1}H NMR_{exptl} {300 MHz, $CDCl_3$, δ (ppm), *J* (Hz)}: 9.32 (d, 1H, J = 8.6), 8.71 (d, 1H, J = 5.7), 6.44 (d, 1H, J = 7.1), 7.00 (m, 1H), 7.45–7.91 (m, 10H, Ar-H).

$[Rh^{III}(2\text{-phpy})_2(q^2)]$ (2). It was prepared by the same procedure of **1** using Hq^2. Orange coloured crystal.Yield: 132 mg (63%). $C_{37}H_{25}N_5OFRh$: Elemental Anal. Calcd.: C, 65.59; H, 3.72; N, 10.34. Found: C, 65.71; H, 3.80; N, 10.32. ESI-MS (CH_2Cl_2): *m/z* 678.1161 $[M + H]^+$. IR_{exptl} (KBr, cm^{-1}) ν: 1479(N=N), 1320, 1252, 1162, 1131, 1101; ^{1}H NMR_{exptl} {300 MHz, $CDCl_3$, δ (ppm), *J* (Hz)}: 9.23 (d, 1H, J = 5.3), 7.94 (d, 1H, J = 6.8), 5.97 (d, 1H, J = 7.6), 6.63 (m, 1H), 6.75–7.84 (m, 10H, Ar-H).

$[Rh^{III}(2\text{-phpy})_2(q^3)]$ (3). It was prepared by the above mentioned procedure using Hq^3. Pink coloured product. Yield: 140 mg (70%). $C_{37}H_{25}N_6O_3Rh$: Elemental Anal. Calcd.: C, 63.08; H, 3.58; N, 11.93. Found: C, 63.25; H, 3.64; N, 11.96. ESI-MS (CH_2Cl_2): *m/z* 705.1091$[M + H]^+$. IR_{exptl} (KBr, cm^{-1}) ν: 1462(N=N), 1328, 1244; ^{1}H NMR_{exptl} {300 MHz, $CDCl_3$, δ (ppm), *J* (Hz)}: 9.24 (d, 1H, J = 5.9), 8.31 (d, 1H, J = 7.8), 5.97 (d, 1H, J = 8.1), 6.82 (m, 1H), 6.93–7.91 (m, 10H, Ar-H).

2.4. Crystallographic studies

The single crystal appropriate for X-ray crystallographic analysis of the complexes **$[Rh(2\text{-phpy})_2(q^1)]$**, **1** and **$[Rh(2\text{-phpy})_2(q^2)]$**, **2** were obtained by diffusion of hexane from dichloromethane of the pure compound. The X-ray intensity data were composed on a Bruker AXS SMART APEX CCD diffractometer (Mo K_α, λ = 0.71073 Å) at 293 K. The detector was located at a distance 6.03 cm from the crystal and total 606 frames were restored with a scan width of 0.3°

in different settings of φ. By using SAINTPLUS and empirical absorption correction was applied using the SADABS package, the data were reduced. Metal atom was placed by Patterson Method and the rest of the non-hydrogen atoms were emerged from consecutive Fourier synthesis. The structures were refined by full matrix least-square procedure on F^2. Anisotropic refinement of all non-hydrogen atoms has been done. The hydrogen atoms were incorporated in calculated positions. All calculations were done using the SHELXTL V 6.14 program package. Molecular structure plots were drawn using the Oak Ridge thermal ellipsoid plot ORTEP. Relevant crystal data are given in Table 1.

2.5. Computational details

The geometrical structures of the singlet ground state (S_0) and the lowest lying triplet excited state (T_1) were optimized in gas phase without any symmetry constraints by the density functional theory (DFT) [36] method with B3LYP exchange correlation functional [37] approach. On the basis of the optimized ground state and excited triplet state geometry structures, the absorption and emission spectra properties in dichloromethane media were calculated by time-dependent density functional theory (TDDFT) approach associated with the conductor-like polarisable continuum model (CPCM) [38]. We computed the lowest 60 singlet − singlet transition and results of the TD calculations were qualitatively very similar. The TDDFT approach had been verified to be reliable for calculating spectral properties of many transition metal complexes [39]. A relativistic effective core potential (ECP) [40] on Rh replaced the inner core electrons leaving the outer core [$(4s)^2(4p)^6$] electrons and the ($4\,d^6$) valence electrons of Rh(III). In the calculation a "double-ξ"quality basis set LANL2DZ was adopted as the basis set for Rh atoms. For H atom we used 6-31G basis set and for C, N and O atoms 6-31 + G(d,p) basis set was used for the optimisation of both the ground state and the lowest lying triplet excited state geometries of all complexes.

Finally (NTO) analysis has been performed for all complexes to understand the nature of excited states involved in absorption and emission processes natural transition orbital. Figures showing MOs, NTOs and the difference density plots were prepared by using the GaussView 5.1 software. All the calculations were performed with the Gaussian 09 software package [41], Gausssum 2.1 program [42] was used to calculate the molecular orbital contributions from groups or atoms.

Table 1
Crystal Data and Structure Refinement Parameters for complexes **1** and **2.**

	$[Rh^{III}(2\text{-phpy})_2(q^1)]$, 1	$[Rh^{III}(2\text{-phpy})_2(q^2)]$, 2
Formula	$C_{37}H_{26}N_5ORh$	$C_{37}H_{25}FN_5ORh$
M_r	647.53	677.53
Crystal system	Triclinic	Monoclinic
Space group	P-1	*C*2/*c*
a/Å	9.645(5)	40.2540(9)
b/Å	15.899(5)	13.5123(3)
c/Å	24.766(5)	27.6551(6)
α/°	76.008(5)	90
β/°	89.907(5)	118.136(1)
γ/°	89.937(5)	90
V/Å^3	3685(2)	13264.7(5)
Z	2	8
D_{calcd}/mg m^{-3}	0.584	1.231
μ/mm^{-1}	0.247	0.550
θ/°	2.5–28.4	3.0–27.6
T/K	293(2)	273
Reflns collected	16988	13682
R1,[a] w*R*2[b] [$I > 2\sigma(I)$]	0.0736(12995), 0.1709(16988)	0.0377(7388), 0.0722(13682)
GOF on F^2	1.101	0.866

[a] $R1 = \Sigma||F_o| - |F_c||/\Sigma|F_o|$.
[b] $wR2 = [\Sigma[w(F_o^2 - F_c^2)^2]/\Sigma[w(F_o^2)^2]]^{1/2}$.

3. Results and discussion

3.1. Syntheses

The substituted 8-hydroxyquinoline Hq^1-Hq^3 as shown in Chart 1 (general abbreviation Hq) were prepared according to the literature procedure [35] and were used as a monoanionic bidentate *N*, *O* donor ligands. In order to vary the photophysical properties of the complexes, the azoaryl groups were introduced at the 5-position of the 8-hydroxyquinoline moiety. It is to be noted that the choice of such ligands helps us to achieve our goal in the context of syntheses of mononuclear rhodium(III) complexes with interesting optical properties.

The stoichiometric reaction of $[Rh(2\text{-phpy})_2Cl]_2$ (2-phpy = 2-phenylpyridine) with appropriate Hq in boiling toluene afforded orange coloured complexes, **1**–**3**, of general formula $[Rh^{III}(2\text{-phpy})_2q]$ in good yield as shown in Scheme 1. Details of the procedures are outlined in the experimental section. The complexes were characterized by IR, ^{1}H NMR, and mass spectroscopy. The spectral data are listed in the syntheses section. The spectra are given in Supplementary information(ESI), IR (Fig. S13, Fig. S14 and Fig. S15), ^{1}H NMR (Fig. S1, Fig. S2 and Fig. S3), and mass (Fig. S4, Fig. S5, Fig. S6) spectra. Notably, the N=N stretching frequencies of **1**–**3** appear at 1460, 1479, 1461 cm^{-1} respectively.

3.2. Molecular geometries

The molecular geometry of $[Rh^{III}(2\text{-phpy})_2(q^1)]$ (**1**) and $[Rh^{III}(2\text{-phpy})_2(q^2)]$ (**2**) has been established by single-crystal X-ray determination. The complex **1** crystallizes in $P2_1/c$ space group and that of complex **2** as *C*2/*c* respectively. The asymmetric unit of complex **1** and **2** consists of two geometrically similar but crystallographically distinct molecules. Molecular view excluding hydrogen atoms is shown in Fig. 1. The numbering of the corresponding atoms in molecules **1** and **2** are, respectively, n and n + 50, e.g., Rh1–O1 and Rh51–O51.

The selected bond distances and angles for complex **1** and **2** are listed in Table S7 and Table S8 in the Supplementary information(ESI), and the molecular views are shown in Fig. 1 for both the complexes.

In complexes **1** and **2** the ligands (Hq^1) and (Hq^2) behave both as *O*, *N* coordinating monoanionic bidentate ligand. The 2-phenylpyridine (2-phpy) moiety adopts commonly an eclipsed configuration. The geometry around the Rh(III) metal centres are distorted octahedral for both the complexes and those are considered by N1-Rh1-N2 bond angle of 175.38(16) for complex **1** and 172.22(9) for complex **2** respectively. For the complex **1,** the Rh1-N1 and Rh1-N2 bond distances emerge at 2.033(4)) and 2.034(4) respectively and that of complex **2** are 2.023(2) and 2.050(2) respectively (Table S7 and Table S8**).**

In summary it is concluded that although the approximate standard deviations for both bond distances and angles are comparatively high the crystal structures confirm the present geometry of the species.

3.3. Geometry optimisation, electronic structure, charge distribution

The diamagnetic nature of the complexes at room temperature representing their singlet ground state t_{2g}^6 configuration. The geometry optimisation for all the complexes at both ground singlet (S_0) and lowest lying excited triplet (T_1) spin state were performed

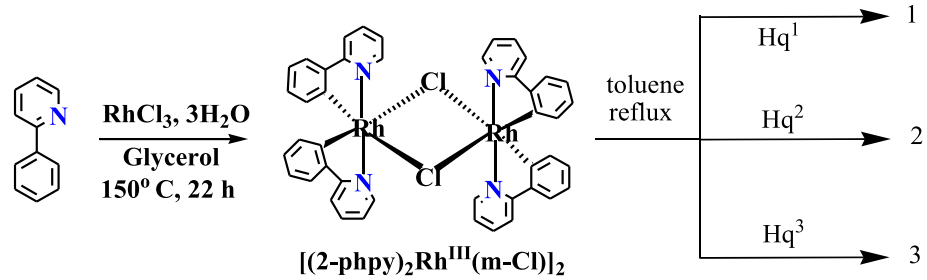

Scheme 1. Synthetic scheme of the reported complexes.

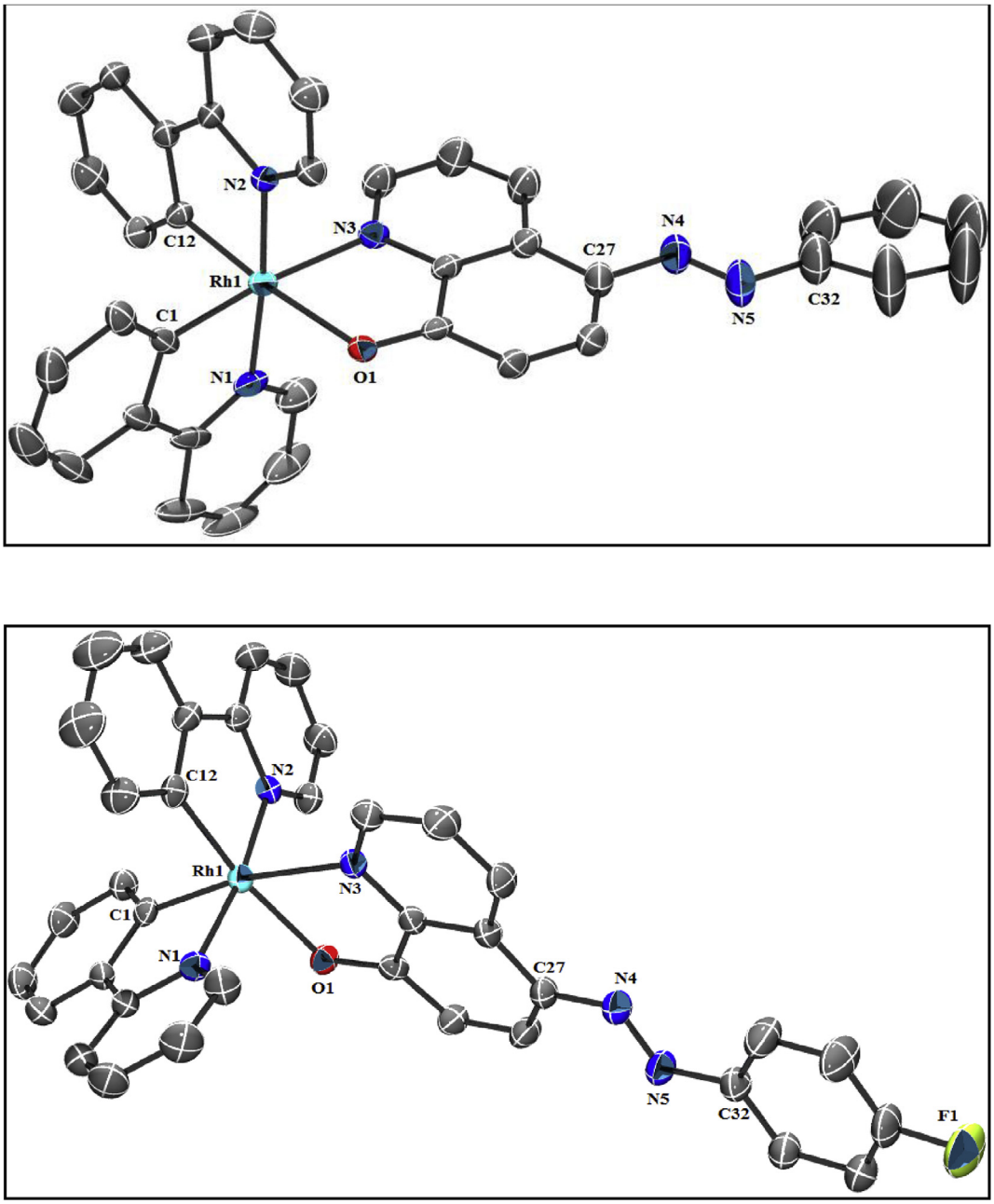

Fig. 1. Top: ORTEP plots (30% probability level) and atom labelling scheme of molecule 1 of complex **1** and bottom: ORTEP plots (30% probability level) and atom labelling scheme of molecule 1 of complex **2**. Hydrogen atoms are omitted for clarity.

in gas phases. The optimized structures of the complex **1** at singlet ground state and triplet excited states are shown in Fig. 2 and Fig. 3 respectively while the same for complex **2** and **3** are given in electronic Supplementary information(ESI) (Fig. S9**,** Fig. S10 and Fig. S11**,** Fig. S12 respectively). The present geometries acquire a distorted octahedral arrangement around the Rh(III) centre. In all complexes the calculated Rh1-C1, Rh1-N3, Rh1-N1, Rh1-O1 bond distances occur near 2.008, 2.243, 2.084, 2.226 respectively for **1** and for **2,** 2.008, 2.243, 2.085, 2.227 respectively and 2.007, 2.248, 2.086, 2.238 Å for complex **3** respectively which are in very good conformity with the experimental values and the slight inconsistency may be due to the crystal lattice deformation existing in actual molecules. Table 2 compare the optimized geometrical parameters of compound **1** in both singlet and triplet state rhodium. The geometrical parameters for both ground and triplet state for other two complexes are given in supplementary information(ESI) [Table S6 and Table S7]. Bond angles are agreed to the same degree of accuracy as bond lengths. The optimized geometries of all the complexes in both S_0 and T_1 states do not show significant differences in the coordination sphere around the rhodium centre corroborates with the similar fashion of binding of the ligands in the complexes.

For all complexes in the ground S_0 state, the ligand moiety (q) is planar and the quinoline moiety ruins *trans* to the aromatic moiety attached to N=N bond which is characterized by the <C32-N5-N4-C27 ≈ 179.902°-179.997° (for complex **1, 2**, **3**). In the triplet excited state (T_1), the geometry around N=N bond is completely different from the geometry observed in the S_0 state. In T_1 state the quinoline moiety become *cis* to the aromatic moiety attached to N=N bond which is also characterized by the <C32-N5-N4-C27 ≈ ~107°-127° (for **1, 2, 3**).

Upon excitation, the complexes experience vertical transition from ground state to singlet excited state and then undergo intersystem crossing to reach the triplet excited state in which emission might occur. According to structure-property relationship, the structural changes would be expected between the S_0 and T_1 states.

The electronic structures calculated by DFT methods are presented in Fig. 2 for ground state and that of triplet excited state in Fig. 3 for 1. For [Rh(2-phpy)$_2$(q)] in this study, the occupied frontier orbitals having contributions from the π-orbital character of the in 2-phenylpyridine (2-phpy) and somewhat from metal d orbital and some extent of π orbital 8-hydroxyquinoline-arylazo ligand (Hq). For instance, for 1 the HOMO consist of 3% of d orbital of Rh(III) and the rest is Hq[1] ligand. The LUMO is totally localized on the π* orbital of Hq[1] ligand. For 2 and 3, the HOMO and LUMO also has almost same contribution as in happened for 1. The contribution of metal d orbital as well as contribution from π orbital of both 2-phpy and Hq ligand in HOMO-1 to HOMO-6 and LUMO+1 to LUMO+6 are given in Table S10 for 1 and Table S3 and Table S4 for 2 and 3 respectively in supplementary information(ESI).

Fig. 4 in main article and Fig. S18 in Supplementary information(ESI) signifies the partial molecular orbital diagram bearing isodensity frontier molecular orbital which are mainly associated with the electronic transitions for complexes and it gives idea of the energy difference between every HOMO and LUMO state.

From isodensity molecular orbital plot and orbital contribution table it is assumed that in all complexes, the electron density in HOMO (H) mainly reside on quinoline moiety including azo group and aromatic system attached to N=N bond along with a minimal metal d orbital (3%). The electron densities of HOMO − 1 for **1, 2** and **3** are mainly associated with metal d and 2-phpy moiety. In HOMO − 2 the electron density resides on mainly Hq ligand for **2** and **3** and for **1** it is for metal d as well as π of 2-phpy ligand. The electron density of HOMO −3 are found at the ligand 2-phpy parts for all the complexes. For HOMO − 4 the electron density engaged in metal d as well as π orbital of 2-phpy for complex **2** and complex **3** and azo part for complex **1.**

In case of unoccupied molecular orbital, i.e, LUMO, the electron density contribution in each LUMO to LUMO+6 state occurring from either π* orbital of 2-phpy ligand or π* orbital of ligand Hq. The metal d-orbital has no role to play in LUMO state for electronic transition for all the three complexes. The energy difference of HOMO and LUMO are −2.87 eV, −2.86 eV and −2.33 eV for the complex **1**, **2** and **3** respectively.

L + 1 of all complexes originates from ligand π* orbital localized on N=N bond, quinoline moiety and aromatic system attached to N=N bond contribution as well as 2-phpy fragment. L + 2 orbital shows a strong contribution of the π* of 2-phpy moiety.

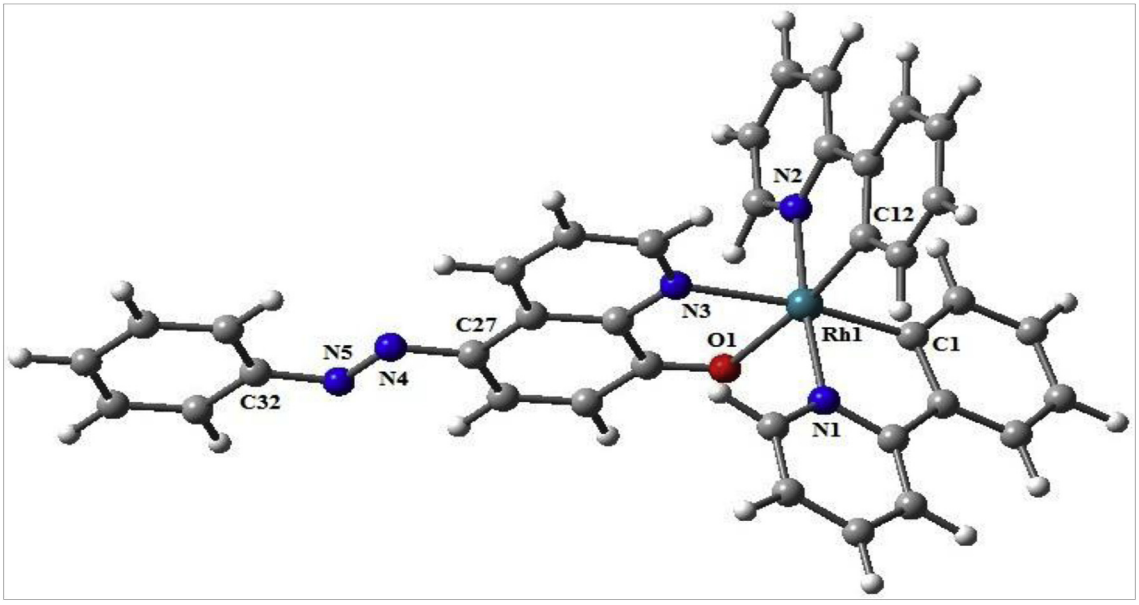

Fig. 2. Ground state optimisation structure of complex **1** in ground state.

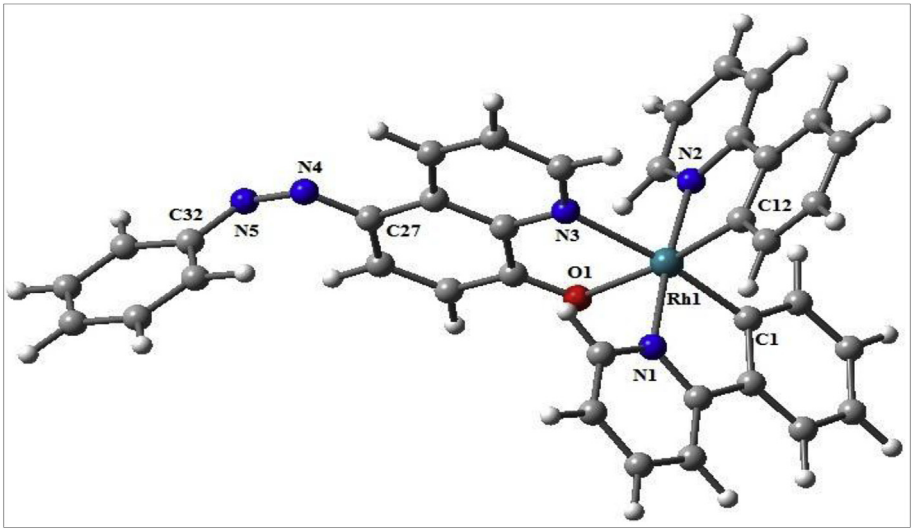

Fig. 3. Triplet state optimisation structure of complex **1.**

Table 2
Comparison of the selected bond lengths (Å) and angles (°) for Complex **1** in both singlet ground state and triplet excited state.

bond lengths				bond angles and dihedral angle			
SINGLET STATE(S_0)		TRIPLET STATE(T_1)		SINGLET STATE(S_0)		TRIPLET STATE(T_1)	
Rh1-N3	2.243	Rh1-N3	2.241	O1-Rh1-N3	75.491	O1-Rh1-N3	75.705
Rh1-O1	2.226	Rh1-O1	2.227	N2-Rh1-C12	80.848	N2-Rh1-C12	80.848
Rh1-N2	2.073	Rh1-N2	2.073	N1-Rh1-C1	80.720	N1-Rh1-C1	80.681
Rh1-C12	2.002	Rh1-C12	2.003	O1-Rh1-C12	172.760	O1-Rh1-C12	172.569
Rh1-N1	2.084	Rh1-N1	2.085	N3-Rh1-C1	171.460	N3-Rh1-C1	171.971
Rh1-C1	2.008	Rh1-C1	2.009	N1-Rh1-N2	175.126	N1-Rh1-N2	175.083
				C27-N4-N5-C32	179.963	C27-N4-N5-C32	107.732

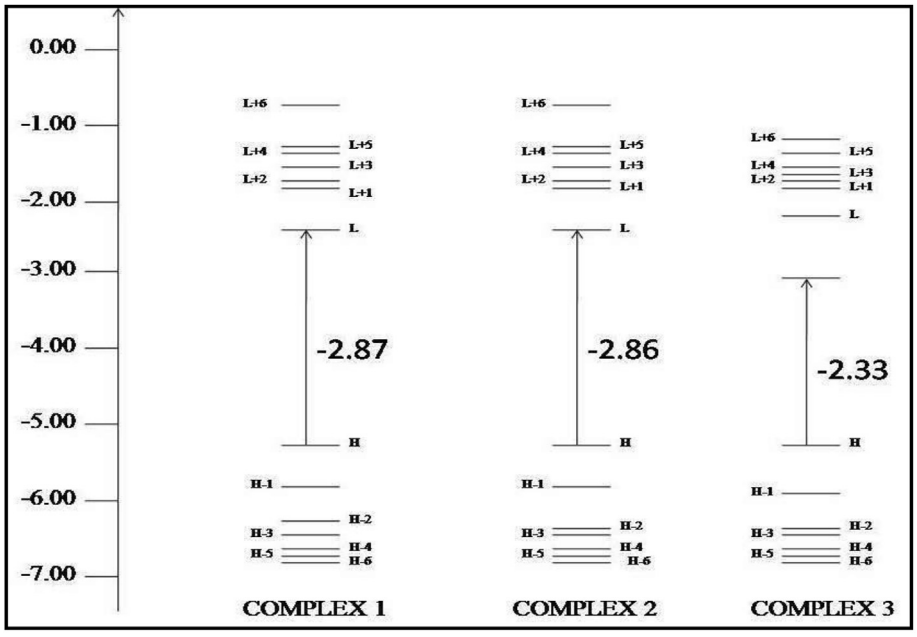

Fig. 4. Partial molecular orbital diagram with some isodensity frontier molecular orbital mainly involved in the electronic transitions for complex **1, 2 and 3**. The arrows indicate the HOMO–LUMO energy gaps. X axis denotes the energy axis with unit eV.

The isodensity surfaces of the Highest and Lowest Singly Occupied Molecular Orbitals, namely HSOMO and LSOMO for all species, at the relaxed T_1 geometry are shown in Fig. 5. Also, the corresponding electrons spin density, which is defined as the difference between α and β spin contributions to the total electron density, are depicted in Fig. 5. The analysis of the singly occupied molecular orbitals at the T_1 geometry showed that the LSOMO is mainly located on the 8-hydroxyquinoline-arylazo moiety and resembles the HOMO of Corresponding S_0 geometry.

On the other hand π orbital of quinoline moiety and N=N bond contributes primarily to HSOMO along with a small contribution arises from the π orbital of the aromatic system attached to N=N bond and some contribution from metal d orbital and HSOMO resembles the corresponding LUMO of the S_0 geometry. The spin density plot at T_1 state for all the complexes illustrates that the spin density is mainly localized on the ligand moiety (hq) thus the lowest-lying triplet excited state (T_1) is the virtually intra ligand (^{3}IL) excited state (ligand-localized) in all complexes.

3.4. Absorption spectral properties

The electronic absorption spectral data and all the parameters for complexes **1**–**3** are summarised in Table 3. The electronic absorption spectra of complexes **1, 2** and **3** in dichloromethane at 298 K are shown in Fig. 6. The electronic absorption spectra of **1, 2, 3** show intense absorption bands at 487–521 nm assigned to mainly intra-ligand or ligand to ligand transition, i.e, ^{1}ILCT/^{1}LLCT, together with less intense low-energy absorption bands and shoulders at *ca.* 396–386 nm which are assigned also to intra-ligand or ligand to ligand transition and another high-energy absorption bands showing at 265–296 nm assigned basically due to metal to ligand transitions. In view of the increased electron density on the rhodium centres due to the phenyl pyridine ligands, the high-energy absorption features are assigned to spin-allowed metal to ligand charge-transfer ^{1}MLCT (dπ(Rh)-π^*(2-phpy)) transitions. On the other hand low energy but high intense absorption bands mainly assigned due to intra ligand or ligand to ligand transition(π(2-phpy)-π^*(2-phpy)) or (π(2-phpy)-π^*(hq)).

In complex 1 three bands occurred at 487 nm ($\varepsilon \approx 58489\ M^{-1}\ cm^{-1}$), 396 nm ($\varepsilon \approx 25614\ M^{-1}\ cm^{-1}$) and 265 nm ($\varepsilon \approx 86494\ M^{-1}\ cm^{-1}$). Whereas for complex **2** these bands are appeared at 491 nm ($\varepsilon \approx 112041\ M^{-1}\ cm^{-1}$), 396 nm ($\varepsilon \approx 13466\ M^{-1}\ cm^{-1}$) and 293 nm ($\varepsilon \approx 57511\ M^{-1}\ cm^{-1}$) respectively and 521 nm ($\varepsilon \approx 38300\ M^{-1}\ cm^{-1}$), 386 nm ($\varepsilon \approx 12819\ M^{-1}\ cm^{-1}$) and 296 nm ($\varepsilon \approx 35120\ M^{-1}\ cm^{-1}$) respectively of uv bands are appeared for complex **3** which are also shown in Table 3. Clearly our aim is to shift the intense lower energy band to a higher wavelength when we go from complex **1** to complex **3**. As for complex **1** the lower energy high intense band occurred at 487 nm as it has only benzene ring in the azo ligand part whereas 491 nm is the transition band appeared for complex **2** and it is somewhat shifted due to electronegative F atom in the benzene ring and its –I effect. The transition band shifted to higher wavelength most, i.e, at 521 nm. In complex **3** due to incorporation of nitro group in the ring and we know –R effect of the group causes the shift.

To understand the nature of the observed UV–vis transitions properties of [Rh(2-phpy)$_2$(q)], theoretical calculations have been

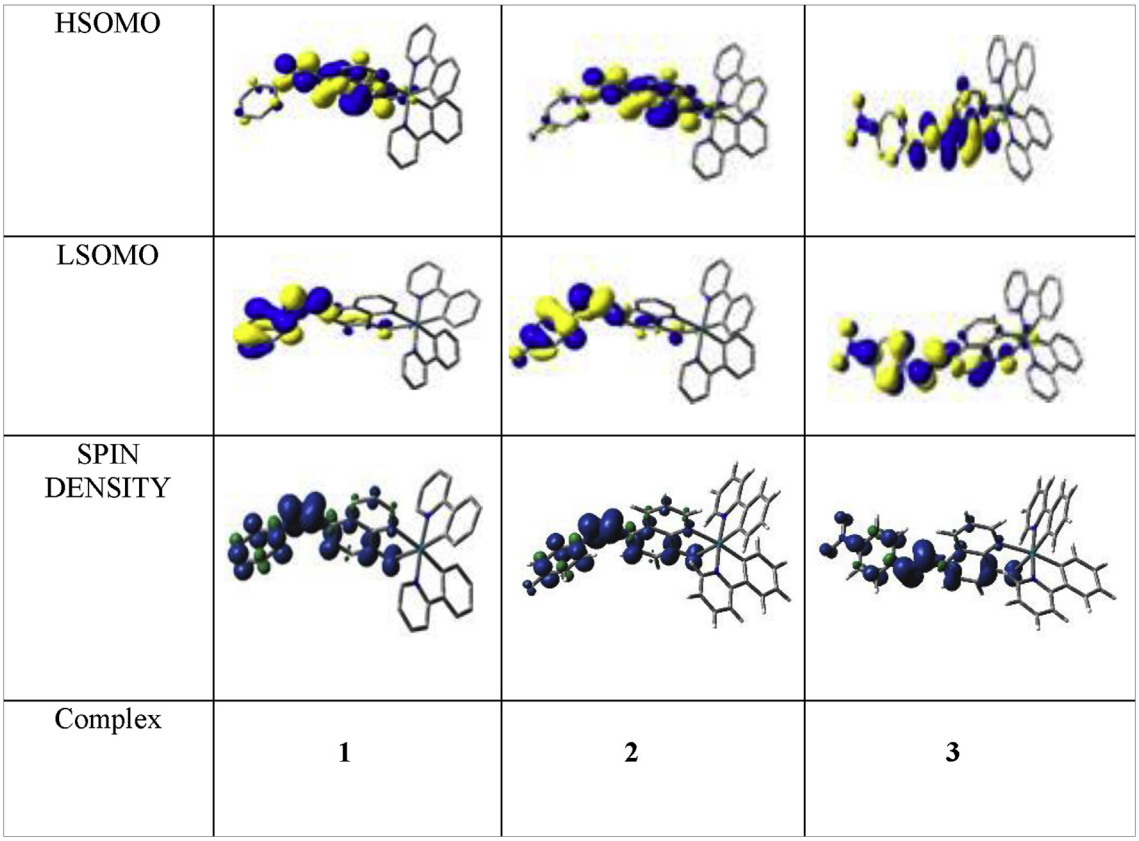

Fig. 5. Isodensity surface plots of the highest and lowest singly occupied molecular orbitals, HSOMO and LSOMO, respectively, along with the corresponding electron spin density, for the complexes **1**, **2** and **3** at their T_1 state geometry. Blue and green colours show regions of positive and negative difference between the alpha and beta electron densities, respectively. (For interpretation of the references to colour in this figure legend, the reader is referred to the Web version of this article.)

Table 3
Photophysical parameters of all the mononuclear complexes in dichloromethane solution at room temperature.

Complex	$\lambda_{max,}$ nm (ε, M^{-1} cm^{-1})	$\lambda_{emi,}$ nm	Φ ($\times 10^{-3}$)	k_r, s^{-1} ($\times 10^{8}$)	k_{nr}, s^{-1} ($\times 10^{9}$)	τ ns
1	487(58489) 396(25614) 265(86494)	560	6.78	1.45	21.24	0.0467
2	491(112041) 396(13466) 293(57511)	580	11.06	12.9	115.77	0.0085
3	521(38300) 386(12819) 296(35120)	615	49.17	2.05	3.96	0.2398

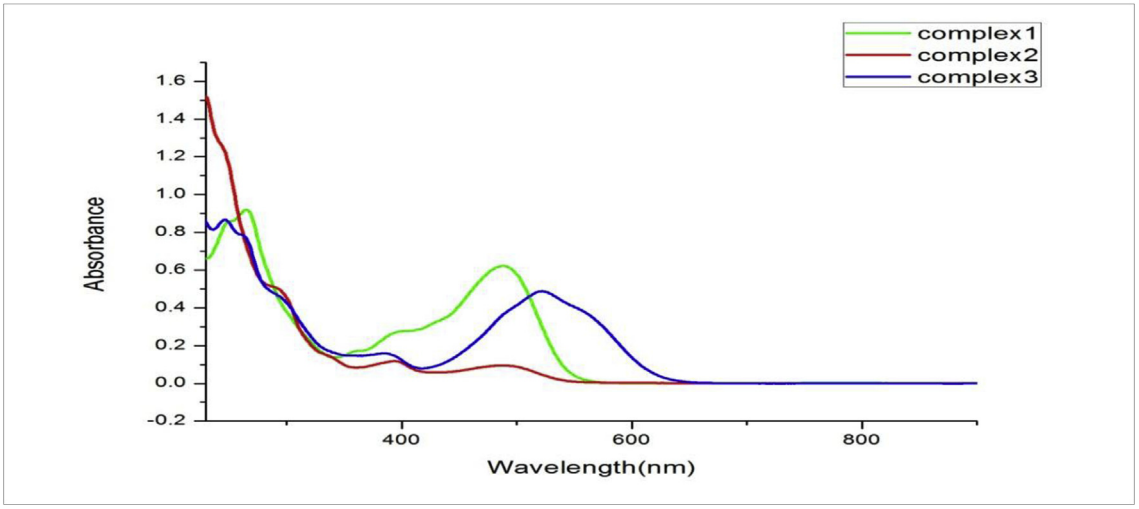

Fig. 6. Absorption Spectra of complexes **1**, **2** and **3** in dichloromethane at room temperature.

conducted. To further rationalize the photophysical properties of complexes **1, 2** and **3** TD-DFT calculations on the corresponding molecular orbitals involved in the transitions were carried out which are depicted in Table S11, Table S5 and Table S6 respectively in electronic Supplementary information(ESI). Fig. 6 shows the experimental UV–Vis spectra and TD-DFT calculated excited states with oscillator strength are in Table S11 for complex **1**, Table S5 and Table S6 respectively for complex **2** and **3** in electronic Supplementary information(ESI). TD-DFT calculations reproduce well with the experimental absorption spectra (curves in Fig. 6**).** For complex **1, 2 and 3**, the lowest energy absorption band (487 nm, 491 nm and 521 nm in Fig. 6) all are assigned mainly to the ILCT or LLCT transition. The low intense low energy bands of complex **1**, **2** and **3**(396 nm, 396 nm and 386 nm respectively are also ILCT or LLCT transition. The higher energy absorptions below 300 nm for all the complexes are too complicated to be resolved. It is basically metal to ligand charge transfer, i.e, MLCT(Rh)→2-phpy or MLCT(Rh)→hq transitions are all included. The calculated absorption energies associated with their oscillator strengths, the main configurations and their assignments as well as the experimental result of **1, 2** and **3** are given in Table S11, Table S5 and Table S6 in electronic Supplementary information(ESI) respectively.

In order to analyze the nature of absorption, we performed an NTO analysis based on the calculated transition density matrices.[40] This method offers the most comprehensive representation of the transition density between the ground and excited states in terms of an expansion into single-particle transitions (hole and electron states for each given excitation).

Here we refer to the unoccupied and occupied NTOs as "electron" and "hole" transition orbitals respectively. Note that NTOs are not the same as virtual and occupied MO pairs from the ground state calculations. Fig. S18 in Supplementary information(ESI) illustrates the natural transition orbitals (NTOs) for complex **1** and those for complex **2** and **3** are given in Supplementary information(ESI) (Fig. S7 and Fig. S8 respectively). Based on our TDDFT NTOs analysis the bands in the region 265–525 nm for all complexes can be characterized as a mixture of MLCT, LLCT and ILCT states.

As illustrated in Fig. S18, optical excitations occur from the occupied (hole) transition orbitals to the unoccupied (electron) transition orbitals. Hole NTOs contributing to the bands are localized on the Rh centre along with π orbital of ligands ($t_{2g} - \pi$) while the electron NTOs are mainly delocalized over the π^*orbital of the ligand moiety.

3.5. Emission spectral properties

The emission spectral behaviour of all the complexes was studied at room temperature in dichloromethane. The photophysical parameters are listed in Table 3. Fig. 7 represents the emission spectra of the complexes in dichloromethane solution.

Upon photo excitation, complexes **1**–**2** display long-lived and low intense greenish-yellow luminescence at 560 nm and 580 nm respectively in DCM solutions at 298 K. In DCM solutions at 298 K, complex **3** display similar but high intense orange emission spectra with maxima at near about 615 nm. These are shown in Table 3.

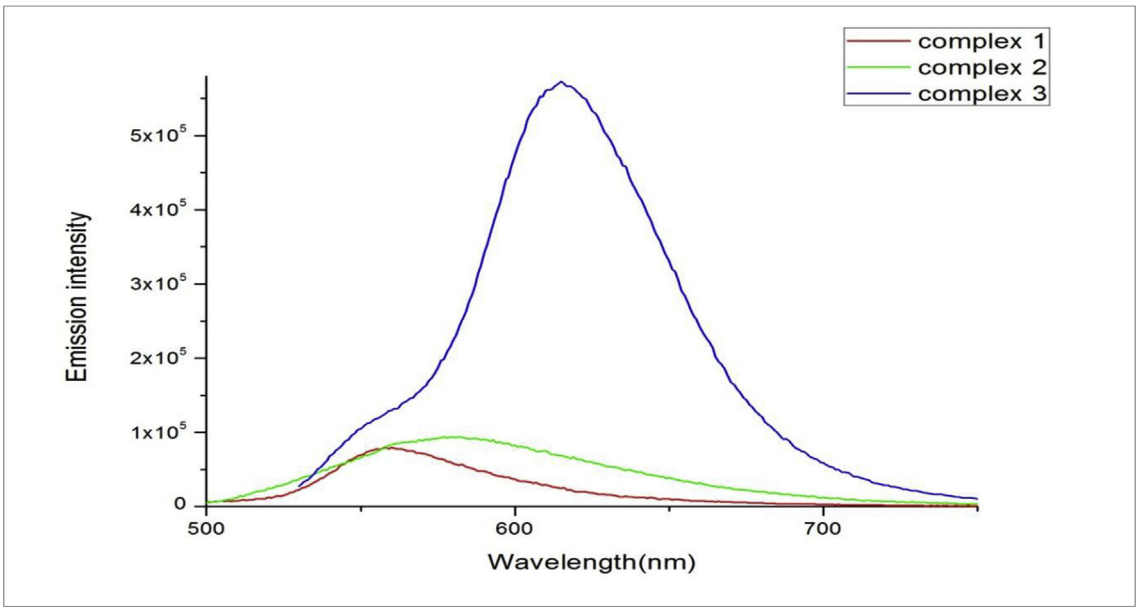

Fig. 7. Emission spectra of complex **1**, **2** and **3** at dichloromethane solution at room temperature.

The photoluminescence property mainly originates from triplet state charge transfer transitions. Table S12 in Supplementary information(ESI) describes the calculated emission energies associated with their oscillator strengths, the main configurations and their assignments as well as the experimental result of complex **1** and **2**, and **3**. It is believed that the change in electronegative atom and group in the aryl azo moiety of the molecule responsible for the fluorescence spectral change as wavelength increases from complex **1** to **3** with the variation of the ligand. In order to elucidate the T_1 states of the complexes from a theoretical perspective, the electron spin density isosurfaces were studied by DFT calculations (Fig. 5). The isosurface of the spin density and HSOMO and LSOMO of complex **1, 2** and **3** is localized mainly on the 8-hydroxyquinoline-arylazo moiety and somewhat on metal (Fig. 5). This is in agreement with the known ^{3}MLCT/^{3}LLCT/^{3}ILCT excited state of cyclometalated Rh(III) complexes.

The photoluminescence property mainly originates from triplet state charge transfer transitions and electron spin density at T_1 state (Fig. 5) reveals the ligand-centered ^{3}IL nature of T_1 state for all complexes. TD-DFT study at T_1 state for all complexes corroborates with mainly the ^{3}ILCT or ^{3}LLCT nature for all the transitions.

In order to analyze the nature of emission, we performed an NTO analysis based on the calculated transition density matrices. Fig. S20 illustrates the natural transition orbitals (NTOs) for all three complexes. Based on our TDDFT NTOs analysis at T_1 state all the bands for complex **1** and **2** and **3** can be characterized as ^{3}MLCT/^{3}ILCT/^{3}LLCT transitions as electron density over metal is very small. As illustrated in Fig. S20, optical excitations occur from the occupied (hole) transition orbitals to the unoccupied (electron) transition orbitals. The hole and electron NTOs contributing to the bands are mainly metal-ligand and ligand localized, respectively.

From the NTO analysis we can see that the electron density of hole predominantly located at the [d(Rh) + π(Hq^1)] for complex **1,** [d(Rh) + π(Hq^2)] for complex **2** and d(Rh) + π(2-phpy) + π(Hq^3) for complex **3** and electron density of unoccupied (electron) transition orbital is mainly locate at π^* orbital of 2-phpy for complex **1** and complex **2** and π^* orbital of Hq^3 for complex **3**. Thus we conclude that emission transition characters are from d(Rh) + π(Hq^1) to π^*(2-phpy) + π^*(Hq^1) for complex **1** and d(Rh) + π(Hq^2) to π^*(2-phpy) + π^*(Hq^2) for complex **2**. In case of complex **3** both hole and electron NTOs contributing to the bands are mainly ligand localized.

At room temperature in solution state the quantum yield value of the complexes are in the range [(6.0–49.0) x 10^{-3}] which are given in Table 3.

Time resolved luminescence spectrum is the measurement of the decay process and the emissive nature of the complexes. Thus time resolved luminescence spectra are recorded for all the complexes. All the complexes display a mono-exponential decay nature and the decay plot for the complex **3** is shown in Fig. 8 while the same plot for other complexes, i.e, for **1** and **2** are given in Supplementary information(ESI) (Fig. S16 & Fig. S17 respectively**).** The fluorescence life time (τ), radiative (k_r) and nonradiative (k_{nr}) decay rate constant are collected in Table 3.

3.6. *Trans→Cis isomerism interpretation by UV–Vis studies*

With UV light or blue light irradiation with particular wavelength to a freely rotating azo moiety of a complex undergoes trans → cis isomerism by rotating of the azo bond very rapidly. The free type azo moiety in a complex thus undergoes rapid trans→cis photoisomerisation and the obtained cis isomer is pretty much stable. By this theory, it have been irradiated all the three trans complexes by passing 450 nm UV light directly to the complex solution for only 5 min and the colour of the ~10^{-5}(N) solution of each complexes has been changed and the compound remained stable for hours and by these transformed solution UV–Vis spectra have been taken and there has been different spectra obtained for all the complexes from the ground state stable trans isomers. Thus it can be concluded that by irradiation with UV light, i.e, hυ to the trans isomer there is a new isomer obtained and this is obviously cis isomer and it is believed to be happened by the free rotation of azo bond by photonic irradiation. The experimental observation matches with the theoretical interpretation. By theoretical point of view, the ground state geometry shows that the all complexes are in trans conformation (Fig. 2) for complex **1** and such incident

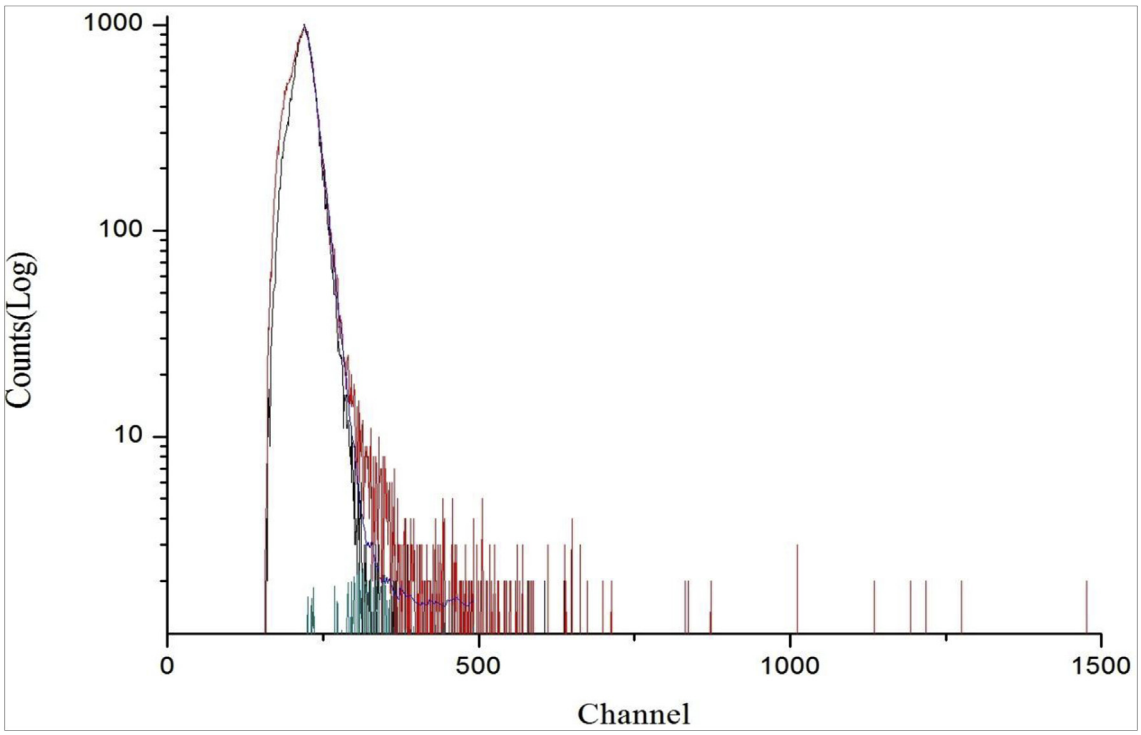

Fig. 8. Changes in the time-resolved photoluminescence decay of complex **1** in dichloromethane at room temperature obtained with 525 nm excitation. The emission at 615 nm was monitored for **3**.

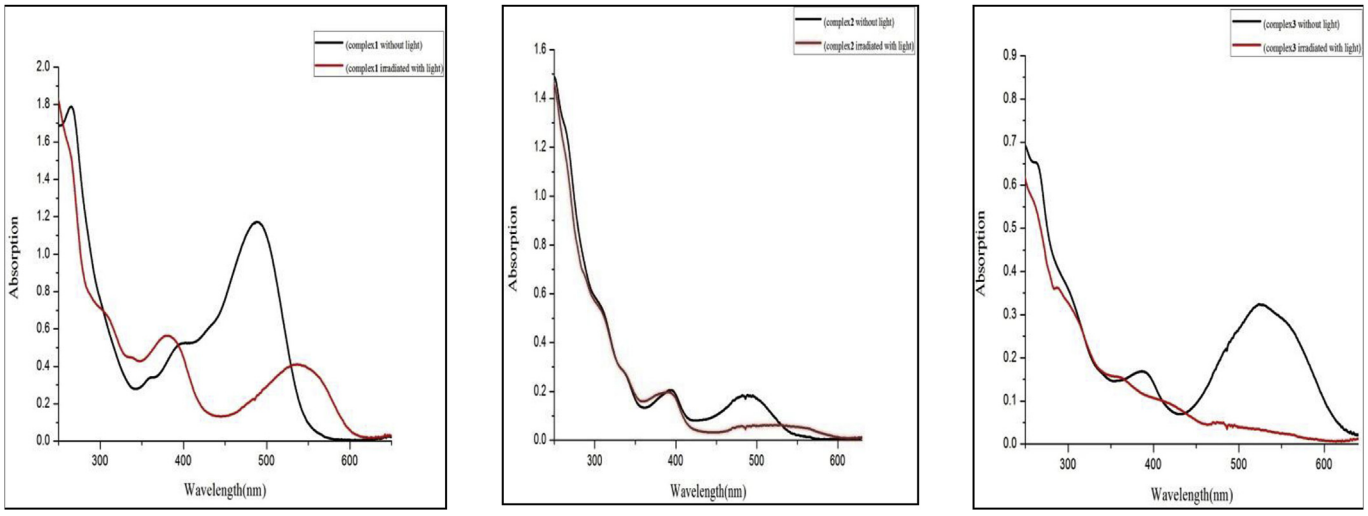

Fig. 9. UV–Vis spectra of complex **1**(Left), complex **2**(middle) and complex **3**(right). The black spectrum is for without light irradiation and red spectrum is for with light irradiation for 5 min of dichloromethane solution at room temperature for each complexes. (For interpretation of the references to colour in this figure legend, the reader is referred to the Web version of this article.)

happened with other two complexes which are given in Supplementary information(ESI). The UV–Vis spectra of both isomer for all the complexes are given in Fig. 9 for complex **1**, **2** and **3** respectively and colour changing images are also given in Fig. 10.

From the UV–Vis spectral changes as well as the changing of the colour of the solution hence prove that probably from the ground state trans isomer after irradiated with photon changes to stable cis isomer and this result correlating the theoretical DFT method.

3.7. Electron paramagnetic resonance (EPR) study for cis-trans isomerism pathway

1–**3** are EPR silent as ^{1}HNMR spectra confirm the diamagnetic nature of all the complexes in parent trans isomer. The colours of

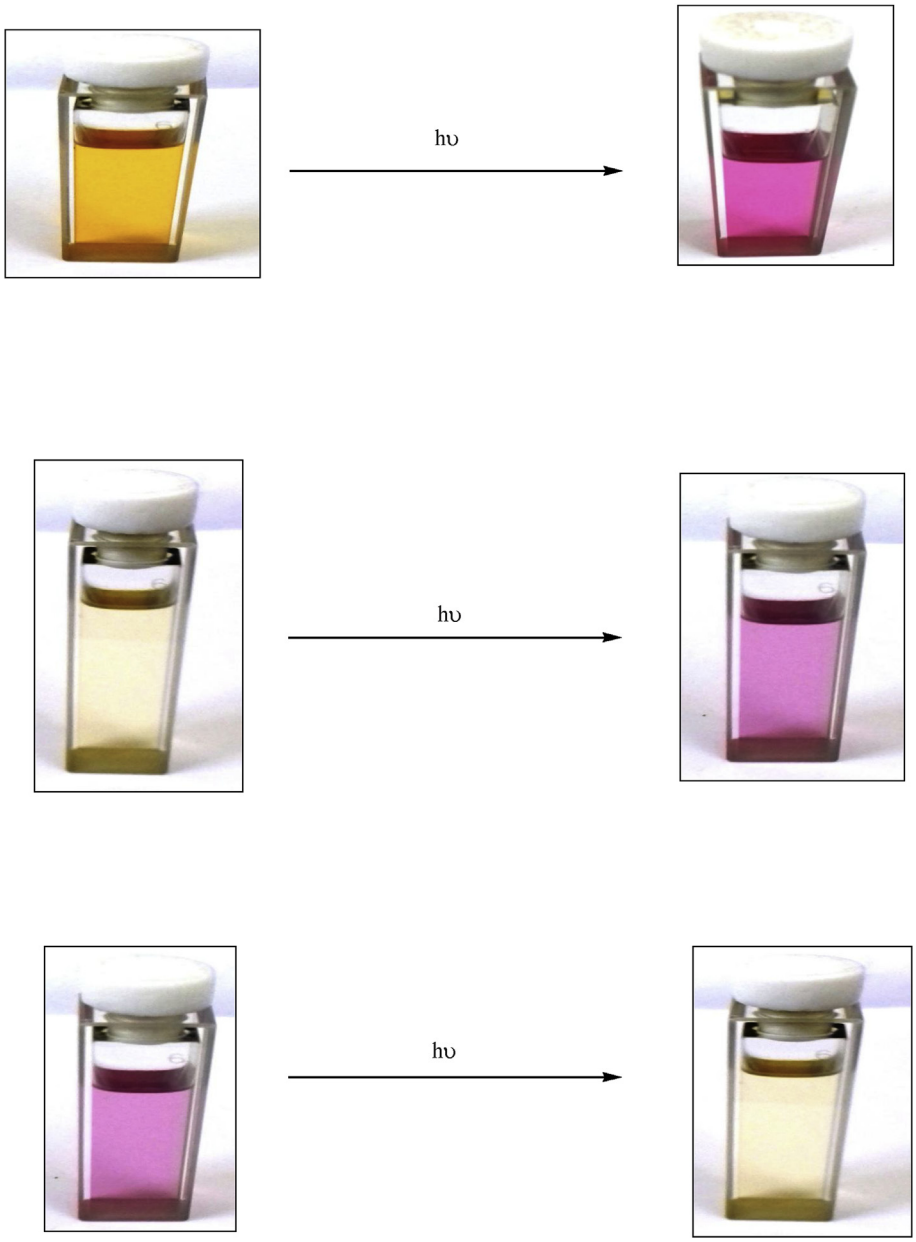

Fig. 10. Images taken before UV light irradiation(left hand side) and images taken after hν irradiation(right hand side) for complex **1**(upper), complex **2**(middle) and complex **3**(below).

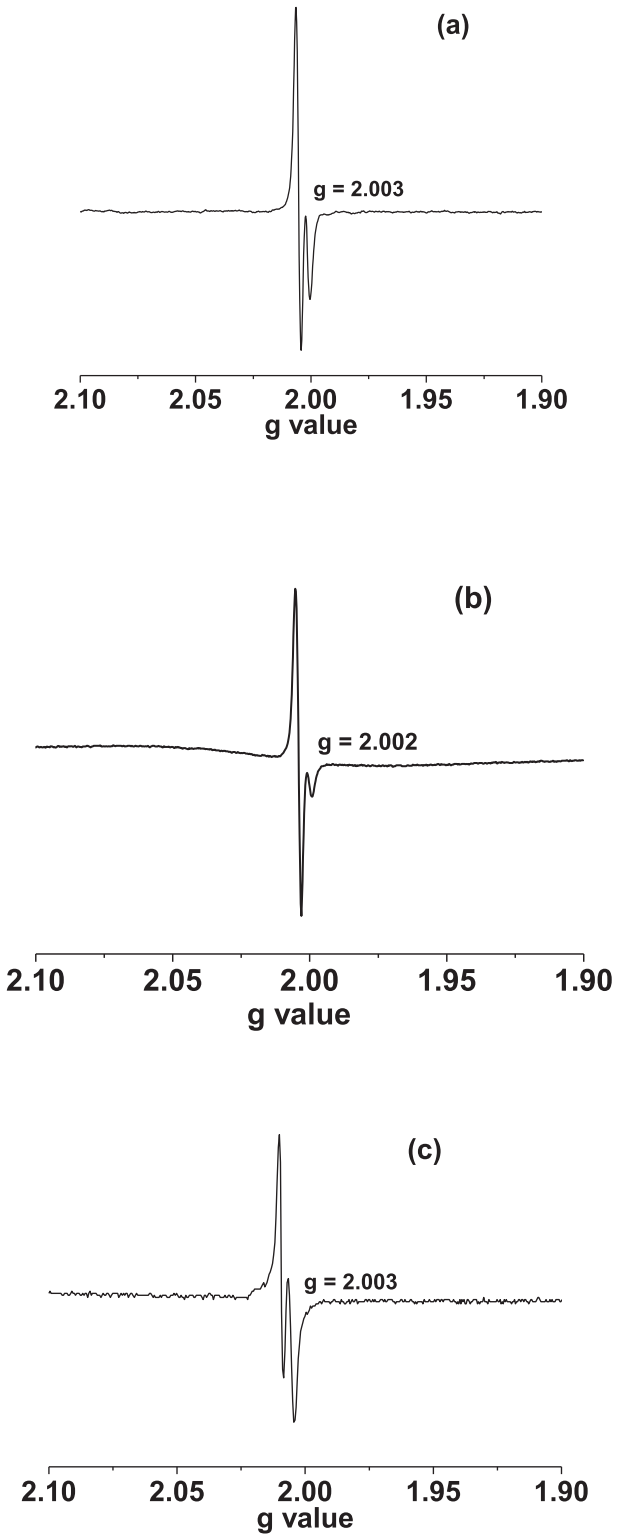

Fig. 11. X-band EPR spectra of (a) **1** (b) **2** and (c) **3** in CH_2Cl_2 at 298 K after irradiation with UV light.

the CH_2Cl_2 solution of the complexes were changed after irradiation with UV light. The bright yellow orange colour of **1** and **2** changed to a pink colour, while pink colour of **3** changed to light yellow. Interestingly, the CH_2Cl_2 solutions of the complexes after irradiation with UV light are EPR active as there is no ^{1}HNMR spectra obtained with that light irradiated complexes, hence prove that the paramagnetic nature. The EPR spectra were recorded at 298 K as shown in Fig. 11. The CH_2Cl_2 solutions give isotropic hyperfine spectra with g values 2.003 that endorse the existence of organic radicals.* The observation authenticates the geometric isomerisation (trans → cis) occurs through a radical pathway.

3.8. Electrochemical studies

Cyclic voltammetry was performed for all the complexes in dichloromethane solution at room temperature under nitrogen atmosphere with tetraethyl ammonium perchlorate (TEAP) as the supporting electrolyte using a Pt electrode as working electrode and the potentials are referenced to the saturated calomel electrode (SCE) without junction correction.

The redox activities of the complexes were investigated by cyclic voltammetry in CH_2Cl_2 at 295 K. The cyclic voltammograms are illustrated in Fig. 12. **1**–**3** exhibit irreversible anodic peaks may be due to the formation of phenoxyl radical state. The anodic peak potentials are 0.94, 0.97 and 0.98 V respectively. The oxidation potential increases from **1** to **3** due to electron withdrawing nature of the aryl group increases from **1** to **3**.

4. Theoretical interpretation of trans-cis isomerism

By theoretical point of view, the ground state geometry shows that the all complexes are in trans conformation which have dihedral angle of around ~179° for all the complexes which were discussed in geometrical optimisation part by DFT calculations. It confirms that the geometry of all the complexes in ground state are in trans conformation with respect to azo moiety. Now On excitation of the complexes, i.e, in singlet excited state optimisation by fixing the dihedral angle near almost 0°, all the trans isomers become to another conformer and these are none other than cis conformers and the dihedral angle changes to $\angle C_{27}$-N_4-N_5-$C_{32} = 12.403°$ for complex **1**, $\angle C_{27}$-N_4-N_5-$C_{32} = 8.179°$ for **2** and $\angle C_{27}$-N_4-N_5-$C_{32} = 17.939°$ for **3** and it give us idea about cis geometrical isomers and all the isomers are shown in Fig. 13.

The UV–Vis spectra of both the conformers for all the complexes are also investigated by means of TDDFT calculations. The ground state time dependent DFT calculation gives the UV–Vis spectra for trans isomers for all the complexes which are same as experimentally obtained UV–Vis spectra of the complexes **1**, **2** and **3** before UV light irradiation. The TDDFT calculation of singlet excited state optimisation geometry (taking the cis optimisation geometry) show almost similar UV–Vis spectrum to that of spectrum of irradiating the sample solution by UV light for all three complexes. The intense absorption peak with wavelength maxima obtained from theoretical TDDFT calculation is ~520 nm which is shown in Fig. 14 which is pretty much closer to the experimental UV–Vis spectrum obtained after UV light irradiation which has absorption maxima at 518 nm for **1** shown in Fig. 9. The UV–Vis spectra of the cis isomers, i.e, uv light irradiated isomers obtained for complexes **2** and **3** by experimentally(Fig. 9) and theoretically(Fig. 14) are matched satisfactorily which have given absorption maxima at about ~490 nm for both complexes proving the existence of cis isomer. This observation from theoretical calculation perspective supported comprehensively the *trans*-cis isomerism. The UV–Vis spectrum of the isomer for complex **1** in excited state obtained theoretically is shown in Fig. 14.

5. Conclusion

In summary, we were synthesized and characterized the [Rh(2-phpy)$_2$q] complexes incorporating bi-coordinating 8-

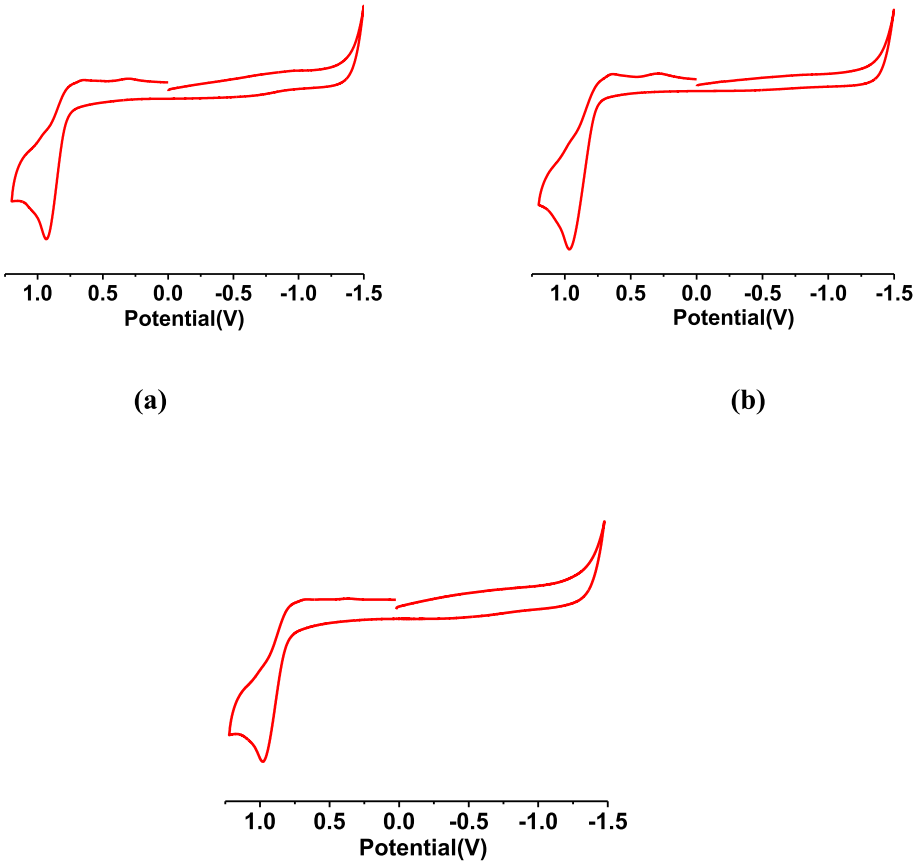

Fig. 12. Cyclic voltammetric diagrams of (**a**) **1**, (**b**) **2** and (**c**) **3** in CH_2Cl_2 at 298 K.

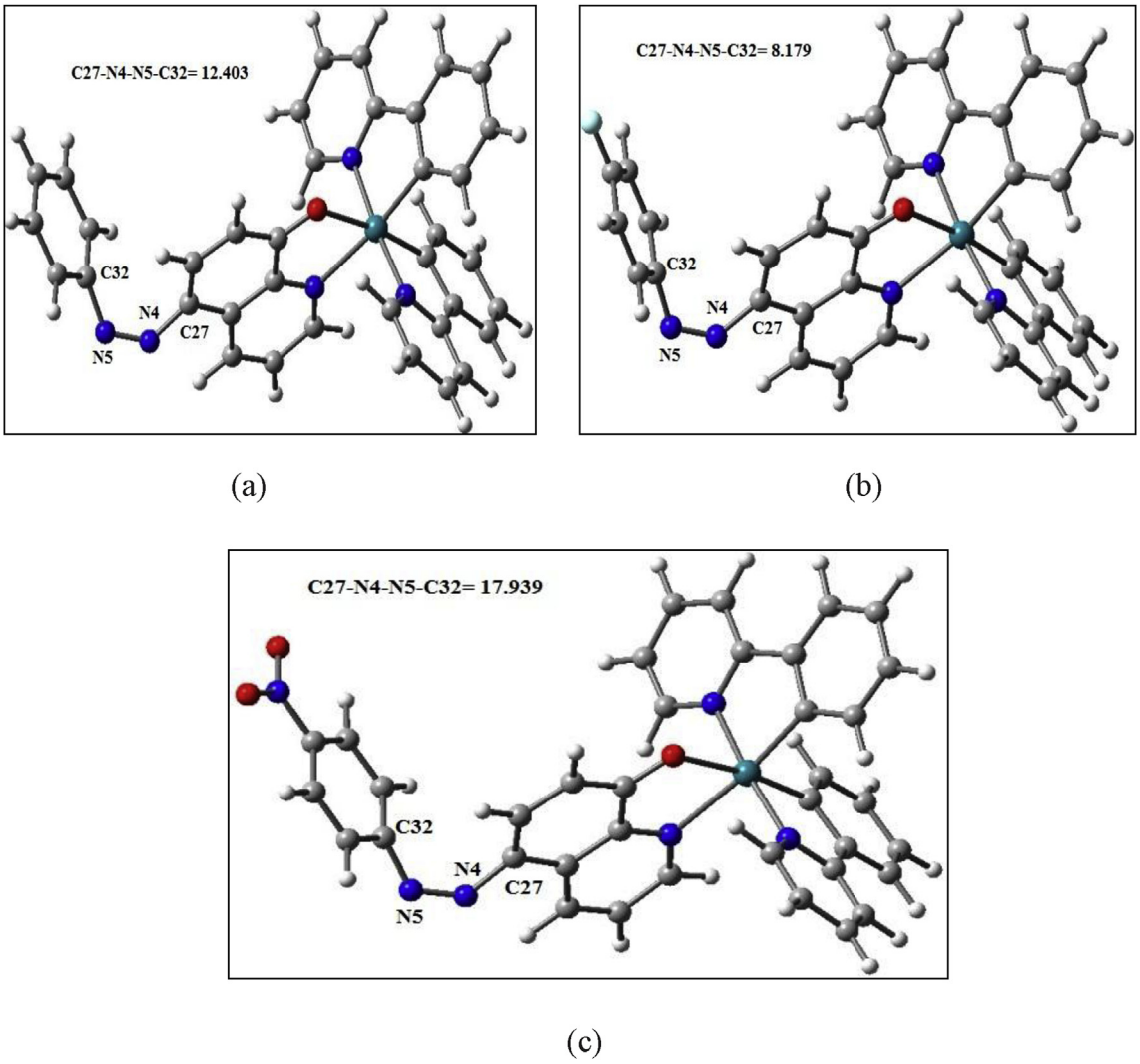

Fig. 13. Optimisation structure obtained from DFT calculations for cis isomers of complex **1** in (a), complex **2** in (b) and complex **3** in (c).

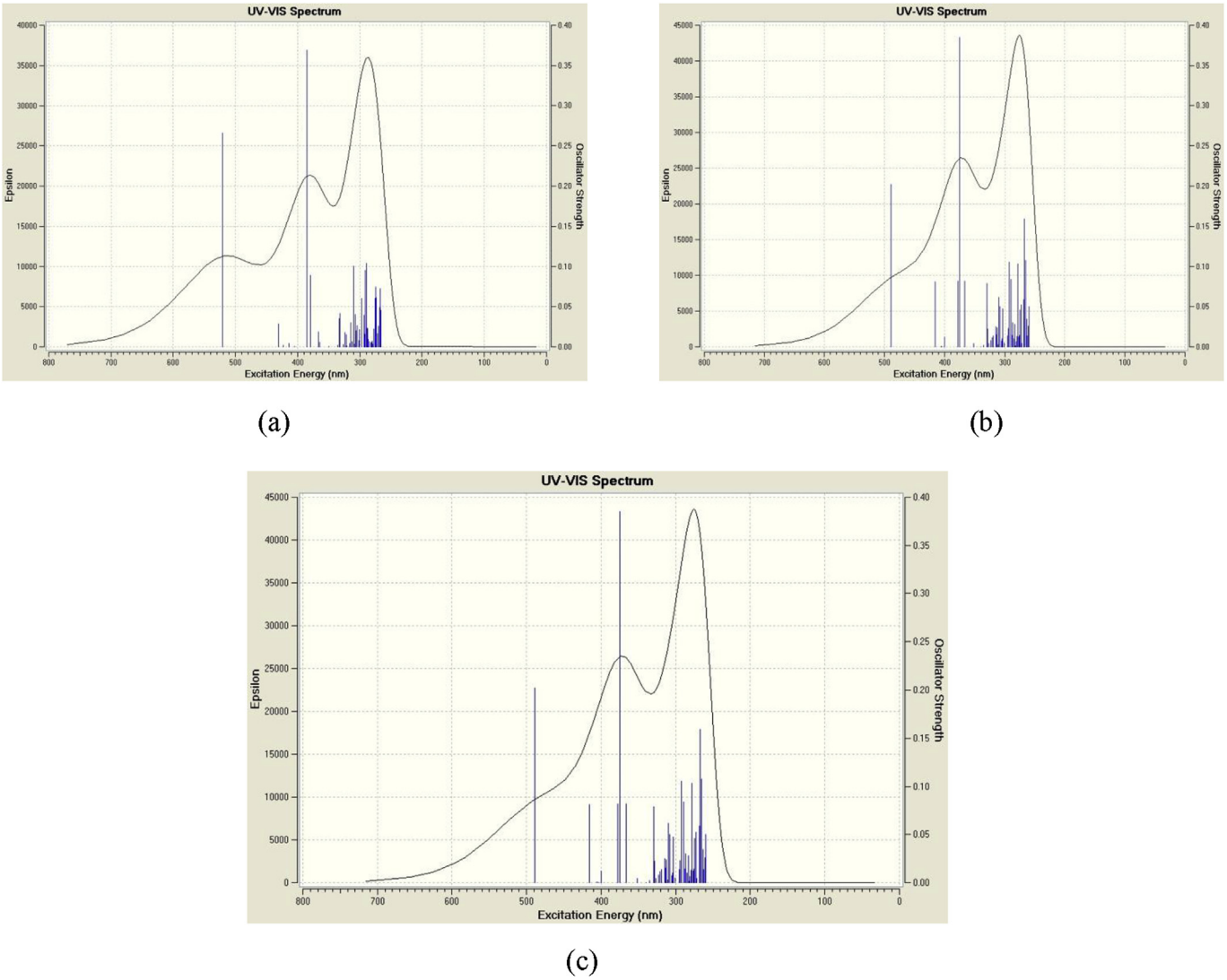

Fig. 14. UV–Vis spectra obtained by TDDFT calculations for cis isomer of the complex **1** in (a), complex **2** in (b) and complex **3** in (c).

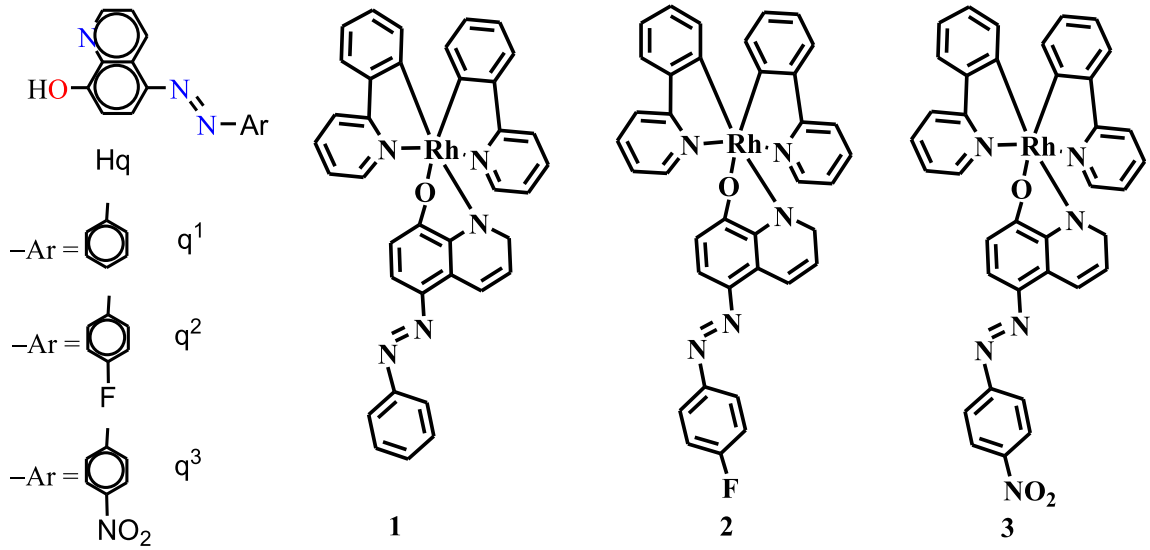

Chart 1. Reported ligands and complexes.

hydroxyquinoline-arylazo ligands. We have performed a comprehensive study of the electronic structure of the complexes. The optimized geometries, energies, frontier orbitals and excited states that emerged from the calculations provided a detailed description of the absorption and emission properties of the complexes. The different Rh(III) species using various O, N coordinating 8-hydroxyquinoline-arylazo ligands along with their theoretical investigations and comparative physicochemical and electrochemical studies were considered comprehensively. It was also investigated how the photoluminescence of the complexes changes by incorporating electron withdrawing group at the ligand centre and the result was very much satisfactory what we expected. The *trans*-cis isomerism studies are carried out by UV light irradiation of the complexes. The isomerisation pathway is also determined by EPR spectroscopic measurement. The *cis*-trans isomerism studies are also done theoretically.

Notes

The authors declare no competing financial interest.

Acknowledgements

Amit Maity is thankful to UGC, New Delhi for the research fellowship. We are thankful to Department of Science and Technology, New Delhi, India for the data collection on the CCD facility setup (Jadvpur University) under DST-FIST program. We also acknowledge CAS, Department of Chemistry, Jadavpur University and DST-PURSE program for other facilities. Financial assistance received from the Science & Engineering Research Board, New Delhi, India is gratefully acknowledged. Thanks to the West Bengal DST board for the financial help.

Appendix A. Supplementary data

Supplementary data to this article can be found online at https://doi.org/10.1016/j.jorganchem.2019.02.012.

References

[1] K.K.-W. Lo, C.-K. Li, K.-W. Lau, N. Zhu, Dalton Trans. (2003) 4682–4689.
[2] W.L. Su, Y.C. Yu, M.C. Tseng, S.P. Wang, W.L. Huang, Dalton Trans. (2007) 3440–3449.
[3] H.-J. Zhong, W. Wang, T.-S. Kang, H. Yan, Y. Yang, L. Xu, Y. Wang, D.-L. Ma, C.-H. Leung, J. Med. Chem. 60 (2017) 497–503.
[4] L.F. Gildea, A.S. Batsanov, J.A.G. Williams, Dalton Trans. 42 (2013) 10388–10393.
[5] C. Wang, H.-C. Lam, N. Zhub, K.M.-C. Wong, Dalton Trans. 44 (2015) 15250.
[6] H.-R. Zhang, Y.-C. Liu, Z.-F. Chen, T. Meng, B.-Q. Zou, Y.-N. Liua, H. Liang, New J. Chem. 40 (2016) 6005–6014.
[7] S. K. Seth, S. Mandal, K. Srikanth, P. Purkayastha, P. Gupta, Eur. J. Inorg. Chem.,10.1002/ejic.201601258.
[8] S.-K. Leung, K.Y. Kwok, K.Y. Zhang, K.K.-W. Lo, Inorg. Chem. 49 (2010). No. 11.
[9] Y. Ohsawa, S. Sprouse, K.A. King, M.K. DeArmond, K.W. Hanck, R.J. Watts, J. Phys. Chem. 91 (1987) 1047–1054.
[10] M.G. Colombo, T.C. Brunold, T. Riedener, H.U. Güdel, M. Förtsch, H. Bürgi, Inorg. Chem. 33 (1994) 545–550.
[11] M.T. Indelli, C. Chiorboli, F. Scandola, Top. Curr. Chem. 280 (2007) 215.
[12] (a) Y. Ohsawa, S. Sprouse, K.A. King, M.K. DeArmond, K.W. Hanck, R.J. Watts, Inorg. Chem. 23 (1984) 1837;
(b) M. Maestri, D. Sandrini, V. Balzani, U. Maeder, A.V. Zelewsky, Inorg. Chem. 26 (1987) 1323;
(c) G. Frei, A. Zilian, A. Raselli, H.U. Güdel, H.-B. Bürgi, Inorg. Chem. 31 (1992) 4766;
(d) G. Calogoro, G. Giuffrida, S. Serroni, V. Ricevuto, S. Campagna, Inorg. Chem. 34 (1995) 541.
[13] Y.J. Su, H.L. Huang, C.L. Li, C.H. Chien, Y.T. Tao, P.T. Chou, S. Datta, R.S. Liu, Adv. Mater. 15 (2003) 884.
[14] C.H. Yang, C.C. Tai, I.W. Sun, J. Mater. Chem. 14 (2004) 947.
[15] E. Holder, B.M.M. Langeveld, U.S. Schubert, Adv. Mater. 17 (2005) 1109.
[16] S.C. Lo, C.P. Shipley, R.N. Bera, R.E. Harding, A.R. Cowley, P.L. Burn, I.D.W. Samuel, Chem. Mater. 18 (2006) 519.
[17] X.M.H. Yu, S. Kwok, W.Y. Wong, G.J. Zhou, Chem. Mater. 18 (2006) 5097.
[18] S. Kume, M. Kurihara, H. Nishihara, Chem. Commun. (2001) 1656–1657.
[19] M. Yamamura, Y. Okazaki, T. Nabeshima, Chem. Commun. 48 (2012) 5724–5726.
[20] A. Hasheminasab, L. Wang, M.B. Dawadi, J. Bass, R.S. Herrick, J.J. Rack, C.J. Ziegler, Dalton Trans. 44 (2015) 15400–15403.
[21] J. Pérez-Miqueo, A. Altube, E. García-Lecina, A. Tron, N.D. McClenaghanc, Z. Freixa, Dalton Trans. 45 (2016) 13726–13741.
[22] T.-T. Yin, Z.-X. Zhao, H.-X. Zhang, RSC Adv. 6 (2016) 79879–79889.
[23] T. Yutaka, I. Mori, K. Masato, J. Mizutani, N. Tamai, T. Kawai, M. Irie, H. Nishihara, Inorg. Chem. 41 (2002) 7143–7150.
[24] M.E. Moustafa, M.S. McCready, R.J. Puddephatt, Organometallics 31 (2012) 6262–6269.
[25] A. Amar, P. Savel, H. Akdas-Kilig, C. Katan, H. Meghezzi, et al., Chem. Eur J. 21 (22) (2015) 8262–8270. Wiley-VCH Verlag.
[26] J. Eng, C. Daniel, J. Phys. Chem. 119 (2015) 10645–10653.
[27] A. Panja, T. Matsuo, S. Nagao, S. Hirota, Inorg. Chem. 50 (2011) 11437.
[28] B.H.M. Dhammika, S.C. Burdette, Chem. Soc. Rev. 41 (2012) 1809–1825.
[29] K.M. Tait, J.A. Parkinson, D.I. Gibson, P.R. Richardson, W.J. Ebenezer, M.G. Hutchings, A.C. Jones, Photochem. Photobiol. Sci. 6 (2007) 1010–1018.
[30] T. Schultz, J. Quenneville, B. Levine, A. Toniolo, T.J. Martínez, S. Lochbrunner, M. Schmitt, J.P. Shaffer, M.Z. Zgierski, A. Stolow, J. Am. Chem. Soc. 125 (2003) 8098–8099.
[31] A. Cembran, F. Bernardi, M. Garavelli, L. Gagliardi, G. Orlandi, J. Am. Chem. Soc. 126 (2004) 3234–3243.
[32] G.L. Tiberio, M.R. Berardi, C. Zannoni, ChemPhysChem 11 (2010) 1018–1028.
[33] M.A.L. Marques, E.K.U. Gross, Annu. Rev. Phys. Chem. 55 (2004) 427–455.
[34] K. Nonoyama, B*ull. Chem. Soc. Jpn.* 47 (1974) 467–468.
[35] M.L. Deda, A. Grisolia, I. Aiello, A. Crispini, M. Ghedini, S. Belviso, M. Amati, F. Lelj, Dalton Trans. (2004) 2424–2431.
[36] R. Czerwieniec, A. Kapturkiewicz, R. Anulewicz-Ostrowska, J. Nowacki, J. Chem. Soc., Dalton Trans. (2001) 2756–2761.
[37] H.C. Zhao, B. Mello, B.-L. Fu, H. Chowdhury, D.J. Szalda, M.-K. Tsai, D.C. nGrills, J. Rochford, Organometallics 32 (2013) 1832–1841.
[38] M.A.L. Marques, E.K.U. Gross, Annu. Rev. Phys. Chem. 55 (2004) 427–455.
[39] Y. Wang, Y. Wang, J. Wang, Y. Liu, Y. Yang, J. Am. Chem. Soc. 131 (2009) 8839–8847.
[40] (a) W. Koch, M.C. Holthausen, A Chemist's Guide to Density Functional Theory, Wiley-VCH, Weinheim, Germany, 2000;
(b) P.J. Hay, W.R. Walt, J. Chem. Phys. 82 (1985) 299.
[41] M.J. Frisch, G.W. Trucks, H.B. Schlegel, G.E. Scuseria, M.A. Robb, J.R. Cheeseman, G. Scalmani, V. Barone, B. Mennucci, G.A. Petersson, H. Nakatsuji, M. Caricato, X. Li, H.P. Hratchian, A.F. Izmaylov, J. Bloino, G. Zheng, J.L. Sonnenberg, M. Hada, M. Ehara, K. Toyota, R. Fukuda, J. Hasegawa, M. Ishida, T. Nakajima, Y. Honda, O. Kitao, H. Nakai, T. Vreven, J.A. Montgomery Jr., J.E. Peralta, F. Ogliaro, M. Bearpark, J.J. Heyd, E. Brothers, K.N. Kudin, V.N. Staroverov, R. Kobayashi, J. Normand, K. Raghavachari, A. Rendell, J.C. Burant, S.S. Iyengar, J. Tomasi, M. Cossi, N. Rega, J.M. Millam, M. Klene, J.E. Knox, J.B. Cross, V. Bakken, C. Adamo, J. Jaramillo, R. Gomperts, R.E. Stratmann, O. Yazyev, A.J. Austin, R. Cammi, C. Pomelli, J.W. Ochterski, R.L. Martin, K. Morokuma, V.G. Zakrzewski, G.A. Voth, P. Salvador, J.J. Dannenberg, S. Dapprich, A.D. Daniels, Ö. Farkas, J.B. Foresman, J.V. Ortiz, J. Cioslowski, D.J. Fox, Gaussian 09, (Revision A.1), Gaussian, Inc., Wallingford, CT, 2009.
[42] E.D. Glendening, A.E. Reed, J.E. Carpenter, F. Weinhold, NBO, Version 3.1, University of, Madison, 1995.